2020 IEEE PES Innovative Smart Grid Technologies Europe (ISGT-Europe) pp. 564–568 DOI: https://doi.org/10.1109/ISGT-Europe47291.2020.9248963

Analysis of the Impact of Synthetic Inertia on Frequency Variations and on Turbine Governor Dead-Bands

D. del Giudice*, A. Brambilla*, S. Grillo* and F. Bizzarri*†
*Politecnico di Milano, Dipartimento di Elettronica, Informazione e Bioingegneria (DEIB)
p.zza Leonardo da Vinci, 32 I-20133 Milano, Italy
Email: {davide.delgiudice, angelo.brambilla, samuele.grillo, federico.bizzarri}@polimi.it
†Advanced Research Center on Electronic Systems for Information and Communication Technologies
E. De Castro (ARCES)
University of Bologna, I-41026 Bologna, Italy

***Abstract*—The increasing penetration of renewable energy sources (RESs) in the set of the production units of power systems is progressively reducing the inertia of those grids. This may result both in excessively large frequency deviations immediately after a power imbalance and in a poor primary frequency regulation. As a consequence, since the crossing of turbine governor dead-bands becomes more likely, generators may be subject to higher mechanical stress and operators may incur in higher O&M costs. To overcome these issues, synthetic inertia has been recently proposed as a potential solution to allow RESs-fuelled generators to improve frequency stability and restore the traditional features of power systems regulation. This paper shows how synthetic inertia can contribute in reducing frequency variations during normal system operation, by considering uncertainty and stochastic load variations. To this end, different scenarios are simulated by using a modified version of the IEEE 14-bus system.**

I. Introduction

Power system frequency deviates from its nominal value every time a power mismatch occurs. In this paper, we distinguish two different instances of a power mismatch: (i) those caused by a severe disturbance (e.g., the trip of a transmission line, of a power plant, etc.) and (ii) those due to relatively small but recurring generation and/or load variations, caused by the volatility of renewable energy sources (RESs), as well as of power demand.

The frequency behavior obtained right after the first class of imbalances happens is known as *inertial response*: its dynamics and eventually the *frequency nadir* are determined by the well-known swing equation [1]–[3]

$$\frac{2H_{\mathrm{COI}}}{f_{\mathrm{s}}}\frac{df}{dt} = P_{\mathrm{m}} - P_{\mathrm{e}},$$

where H_{COI} is the inertia constant of the equivalent center of inertia (COI), df/dt is the rate of change of frequency (ROCOF) of the system, f_{s} is the nominal frequency, and P_{m} and P_{e} are respectively the power provided by the prime mover and the output power of the equivalent generator. The inertia constant, given by the whole set of the rotating masses of the synchronous generators connected to the grid, plays a crucial role: the higher such parameter, the lower the rate of change of frequency in the inertial response.

On the contrary, the second class of imbalances can be considered as stochastic power variations characterised by a zero mean value and a given variance. On average, such variations may balance each other in a relatively short amount of time. They cause relatively small and random fluctuations in grid frequency [4], [5].

Dead-bands are added to turbine governors (TGs) to prevent them from continuously varying the mechanical power that drives the synchronous generators in case of small—but recurring—frequency deviations, with the aim to reduce mechanical stress and O&M costs of TGs [2].

If on the one hand the first class of imbalances has been widely analyzed and studied in literature—mainly due to the impacts that these events may have on power systems—, on the other hand only recently the effects of the second class of imbalances—which is the focus of this paper—have started to be addressed by thorough studies [6], [7].

In the recent years, power grids have been experiencing significant changes caused by the increasing penetration of RESs [8]. The consequent decreasing trend in system inertia, conventional generation and frequency control services is leading to deeper frequency nadirs following severe power mismatches and more frequent dead-band crossings of the TGs when stochastic power fluctuations are considered, which makes the implementation of dead-bands ineffective. This ultimately results in an increased tear-and-wear of TGs, as reported in [2]. RESs-fuelled generators are typically incapable of providing inertia due to two main reasons: (i) they may lack of rotating masses whose kinetic energy could be exploited during the inertial response (e.g., photovoltaic plants); (ii) they are connected to the grid through converters whose control is aimed at attaining a given active and reactive power output, regardless of grid conditions. Thus, such generators cannot provide inertia, even if they had any.

In order to cope with the reduction in power system inertia, the so-called synthetic (or virtual) inertia has been introduced in the recent years [9]. This concept entails a new control strategy for converter-connected generation, where the ROCOF and the frequency deviations are measured and used as an input in a control scheme to regulate the power

output of RESs-fuelled generators so that they can participate to frequency regulation according to the designed control [10], [11]. Contrary to synchronous generators, RESs-fuelled generators providing synthetic inertia do not need any dead-band to limit mechanical stress and can improve frequency stability through a fast intervention because the bandwidth of their controllers can be significantly larger than the nominal frequency of the system.

In [6], Authors state that "Demanding renewables participation in frequency response on a continuous basis could be one of such measures [to limit the substantial increase of the RMS frequency deviation, *ed*]." The aim of the present paper is to prove that this statement is correct and that the implementation of synthetic inertia on inverter-interfaced RESs can effectively limit the frequency deviations caused by stochastically-varying loads. Furthermore, as shown later on in the paper, this achievement results in a reduced activation rate of TGs dead-bands and, thus, lower mechanical stress and O&M costs.

In this paper, an equivalent photovoltaic (PV) plant is connected to a test system through an inverter equipped with a control strategy implementing synthetic inertia. We describe the proposed controller and assess the impact of synthetic inertia on TG dead-bands and frequency variations by simulating the connection of a stochastically-varying load.

II. Simulation setting

A. Test system

As test benchmark we use the well known IEEE 14-bus system (largely used in literature [12], [13]), which includes automatic voltage regulators (AVRs) for each generator and a TG for generators 1 and 2 only. The test system data can be found in [14], [15] and the one-line diagram is reported in Fig. 1. With respect to the base-case model,

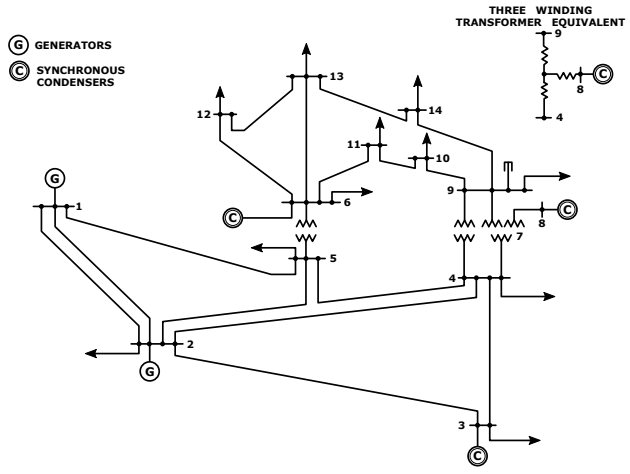

Fig. 1. One-line diagram of the IEEE 14-bus system.

36 mHz dead-bands are implemented in TGs and a randomly variable load, modelled as a Gaussian process with zero mean and 1 MW variance, is added to BUS-13 [16]. The numerical value of the dead-band has been chosen in order to comply with the standards in [2]. Moreover, a 2 MW PV power plant is connected to BUS-11. In comparison with the other generators already existing in the grid (670 MW), the power rating of such plant is decidedly low. This was done on purpose, in order to show that the exploitation of even a small RES-fuelled generator and its DC bus voltage may result in a significant improvement in frequency regulation.

B. Control scheme for the implementation of synthetic inertia

The block schematic of the PV system is depicted in Fig. 2. The numerical values of the parameters are reported in Table I.

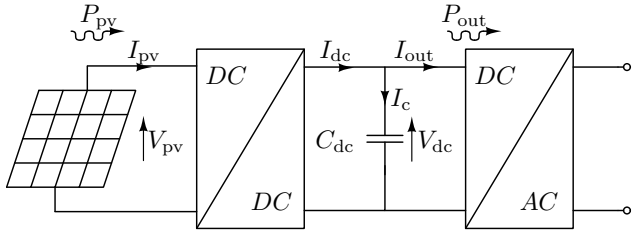

Fig. 2. The PV power plant connection scheme.

TABLE I
NUMERICAL VALUES OF THE PARAMETERS OF THE SCHEME IN FIG. 2. THE SUPERSCRIPT "REF" DENOTES THE REFERENCE PV PLANT OPERATING CONDITIONS CONSIDERED DURING SIMULATION. THE VALUE OF DC-LINK CAPACITANCE CAN BE OBTAINED BY INSTALLING A SUPERCAPACITOR.

V_{pv}^{ref}	700 V
I_{pv}^{ref}	2.8571 kA
V_{dc}^{ref}	680 V
C_{dc}	43 F

Since the main focus of this paper is to analyze the overall effects of synthetic inertia on frequency variations and on TGs, behavioral functional models of DC/DC and DC/AC converters are adopted for the sake of simplicity. The former is controlled so that the PV plant always works as close as possible to the maximum power point, while the latter provides synthetic inertia and controls the capacitor voltage at the DC bus[1]. Moreover, rather than using the output of a phase-locked loop, the frequency of the COI f_{COI} is assumed to be known and available to synchronize the DC/AC converter to the grid [17].

When RESs-fuelled generators do not contribute to frequency control, the behavior of f_{COI} after a power imbalance P_{imb} (i.e., the difference between power generation P_g and demand P_l) is approximately regulated by the block diagram depicted in Fig. 3. As a consequence, the frequency dynamic is strictly determined by H_{COI} (the overall electric power system inertia), D_{COI} (load damping), and, provided that f_{COI} exceeds a given dead-band, also by primary frequency regulation, which can be modelled as a low-pass filter with gain K and time constant τ.

The controller used in this paper to implement synthetic inertia complemented with the block schematic of the power

[1]In our behavioral model we use a capacitor (supercap) to store energy; in detailed implementation the capacitor can be substituted by a suitable energy-rated storage system.

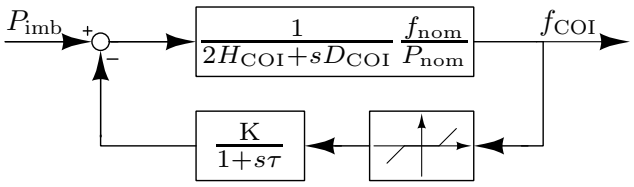

Fig. 3. Block diagram describing the behavior of grid frequency following a power imbalance in a traditional electric power system (i.e., without the implementation of synthetic inertia).

system is depicted in Fig. 4. Its behavior can be described as follows.

① Following a power imbalance $P_{\rm imb}$, a frequency deviation $\Delta f_{\rm COI}$ is detected.
② The signal $\Delta f_{\rm COI}$ is fed to a P (proportional) controller, whose output is a change in the reference DC bus voltage $\Delta V_{\rm dc}^{\rm ref}$.
③ A PI (proportional-integral) controller compares the new voltage set-point ($V_{\rm dc}^{\rm ref}+\Delta V_{\rm dc}^{\rm ref}$) and the DC bus voltage ($V_{\rm dc}$), giving as output the capacitor current $I_{\rm c}$.
④ This current is subtracted to that provided by the DC/DC converter ($I_{\rm dc}$), providing as output the current $I_{\rm out}$.
⑤ The product between $I_{\rm out}$ and $V_{\rm dc}$ is the power entering the DC/AC converter ($P_{\rm out}$).

By adopting this scheme, the power output of the converter depends on frequency and the behavior of synchronous generators during the inertial response can be mimicked.

The parameters of P and PI controllers, listed in Fig. 4, are tuned by considering the linearization of the PV system around the reference operating conditions described in Fig. 2 and by assuming that dead-bands of TGs were not crossed (i.e., primary frequency regulation is absent). In both controllers, a saturation block is added to keep the voltage and the current of the capacitor within security limits. The $\Delta V_{\rm dc}$ maximum allowed capacitor voltage variations were set to $\Delta V_{\rm dc}=\pm 0.1 V_{\rm dc}^{\rm ref}$, while the capacitor current could not exceed in module $1\,\mathrm{kA}$. In order to avoid interferences between control and commutation, the parameters of the PI controller were tuned to obtain a closed-loop cutoff frequency at least 10 times smaller than the switching frequency of the DC/AC converter. Lastly, the P controller gain was designed to achieve power variations comparable with those of the stochastic load connected to the grid. This is a relevant aspect better detailed in the following.

Fig. 5 depicts the frequency and PV power output variation after a $1\,\mathrm{MW}$ power imbalance at $t=1\,\mathrm{s}$ and by considering the control scheme of Fig. 4. The upper panel shows that the implementation of synthetic inertia allows to reduce the rate of change of frequency after a power mismatch, while keeping its steady-state value unaltered. As shown in the lower panel, the proposed control scheme requires the output power to rapidly change. In particular, the original power injection ($2\,\mathrm{MW}$) is restored as soon as frequency reaches steady-state.

The synthetic inertia control has been tuned to compensate a $1\,\mathrm{MW}$ disturbance, which, if compared to the power rating of the IEEE 14-bus test system, constitutes a small disturbance. Nonetheless, if we consider a massive exploitation of RESs-fuelled generators equipped with synthetic inertia, it would be possible to limit frequency variations not only in case of stochastic load variations, but also following severe contingencies. However, this would require an additional coordination among the converter controls installed in each plant.

In general, the main design parameters to consider for the implementation of synthetic inertia in a single plant are the maximum power and energy variations (positive and negative) that can be provided after a power mismatch, which in our case are respectively equal to $\pm 1\,\mathrm{MW}$ and $\frac{1}{2}C\left(\Delta V_{\rm dc}^2 \pm V_{\rm dc}^{\rm ref}\Delta V_{\rm dc}\right)$. When these limits are exceeded, the controller providing synthetic inertia saturates because it cannot modify power and energy any further to compensate the power imbalance. If this happens, the plant stops providing frequency regulation.

III. Simulation results

The dynamic behavior of the modified IEEE 14-bus system is simulated under different scenarios with random load step variations, which implement the stochastically-varying load. These scenarios consider the presence or absence of dead-bands in TGs and of synthetic inertia. Simulations were performed with simulator PAN [18], [19].

We assume that the power system model is stable, ergodic and stationary. An analytic solution of the Fokker-Planck equation to derive the average value and variance of the frequency variations is impossible due to the non-linear characteristics of power system components. We thus simulate the IEEE 14-bus system for a 6-hour time interval where at every $1\,\mathrm{s}$ we apply a power step variation and each step is linearly applied in a time interval of $10\,\mathrm{ms}$. This leads to 21600 power steps. Such a high number of steps, together with the assumed load profile and system properties, constitutes a reasonable baseline for making a statistical analysis of the rotor speed of the generators and, thus, of grid frequency. We model the load variation as a box-car waveform generated by a zero mean, unit variance Gaussian white noise stochastic process colored by a low pass-filter, described by the Ornstein-Uhlenbeck process

$$d\eta_t = \alpha\left(\mu-\eta_t\right)dt + b\xi dt,$$

where $\mu=0$, $\alpha=0.5$ (load reversal time), ξ is the white noise. The samples of the η_t random variables are generated according to the mean and variance of the Ornstein-Uhlenbeck Gaussian process. η_t is thus transformed in a discrete box-car function on the $1\,\mathrm{s}$ evenly spaced time grid [7], [12], [20]. Since the η_t samples can be computed before starting the simulation, we actually solve a random differential equation.

In the introduction of [6] it is stated that: "Inertia is shown to have little effect on the RMS frequency deviation, contrary to its role in transient frequency response to contingencies". We show that such statement does not apply to *synthetic* inertia. To this end, for each analysed scenario we show the corresponding frequency $f_{\rm G1}$ histogram of the largest generating unit G1, which constitutes an aggregate indicator of frequency deviations. The histograms are normalized so that a uniform bin width is used, i.e., all bins of the same histogram have equal width, and the heights of each

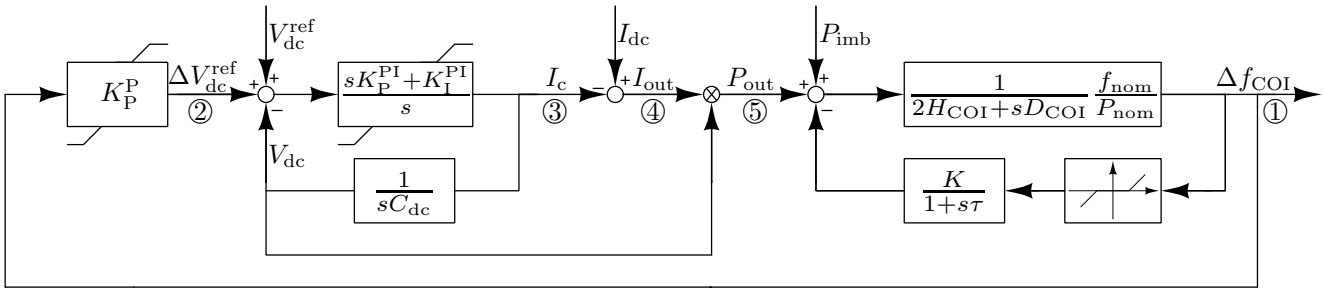

Fig. 4. Block diagram describing the behavior of grid frequency after a power imbalance when the PV plant is equipped with a converter providing synthetic inertia. $K_{\mathrm{P}}^{\mathrm{P}} = 2121$, $K_{\mathrm{P}}^{\mathrm{PI}} = 8600$, $K_{\mathrm{I}}^{\mathrm{PI}} = 671875$ (the superscript refers to the P and PI controllers, while the subscript refers to the proportional (P) or integral (I) gains of these controllers).

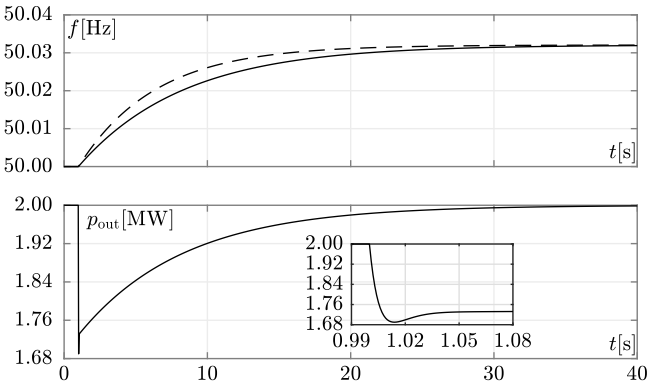

Fig. 5. Upper panel: frequency variation following a 1 MW power imbalance with (dashed line) and without (solid line) synthetic inertia. Lower panel: PV power output variations after the same power mismatch with synthetic inertia, with an inset around 1 s.

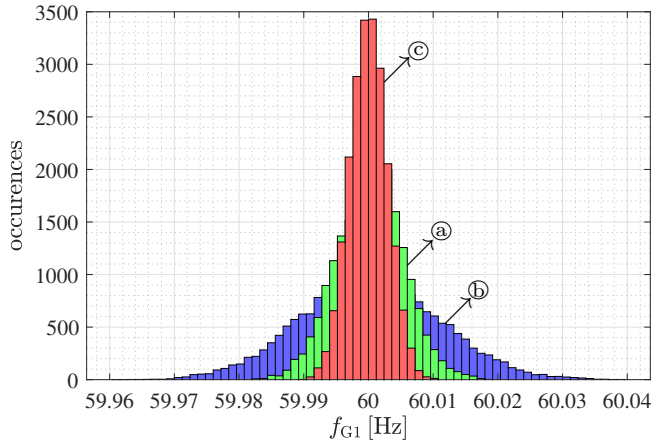

Fig. 6. Histograms of the frequency variations. The green histogram ⓐ refers to the scenario with *no dead-bands* of TGs and with *no synthetic inertia*. The blue histogram ⓑ refers to the case with *dead-bands* and with *no synthetic inertia*. The red histogram ⓒ refers to the scenario with *dead-bands* and *synthetic inertia*.

histogram count the number of occurrences of frequency variations in the bins.

We initially performed a reference simulation of the IEEE 14-bus power system with nominal values of parameters and *without any dead-band* and *synthetic inertia*. In this case TGs continuously modify the power of the prime mover to limit frequency variations. The frequency histogram obtained in this scenario is shown in Fig. 6 (green, ⓐ). The second simulation was carried out by considering dead-bands, which are typically added to prevent the relentless operation of TGs. Their insertion exposes the IEEE 14-bus power system to larger frequency variations (see Eq. 14 of [6]), since TGs intervene by modifying the power of the prime mover only when dead-bands are exceeded. The frequency histogram is shown in Fig. 6 (blue, ⓑ) together with those of other scenarios to allow an easy comparison. In this case, the lower and upper tails of the histogram extend till 60 ± 0.036 Hz, i.e., the frequency limits of dead-band. This means that we have sporadic interventions of the TGs. In the third scenario we activated the PV synthetic inertia control and repeated the simulations. The obtained frequency histogram is reported in Fig. 6 (red, ⓒ). In this case, the occurrences of frequency variations fall in a narrower frequency interval around 60 Hz, which completely prevents the activation of TGs throughout the whole simulation time. The action of the synthetic inertia is based on the fast accessibility to a storage device (i.e., the DC bus supercapacitor), which exchanges power with the grid while the power generated by the solar array remains the same. The frequency extension of the bins depends on the amount of stored energy available to yield synthetic inertia. The larger the available energy, the narrower the frequency extension. This is in the obvious direction of increasing the number of RESs equipped with synthetic inertia capabilities connected to the grid.

The controller shown in Fig. 4 checks the upper/lower voltage and current limits of the DC-bus capacitor and provides synthetic inertia as long as such limits are not exceeded. Consider for instance Fig. 7, which depicts the DC-bus voltage V_{dc} obtained in the simulation scenario where synthetic inertia is activated. In this plot, the capacitor voltage changes over time but always remains inside the given limits. To have a clear picture of what happens when dead-bands of TGs are introduced in a power system, we increase the variance of the stochastic load to 10 MW and perform a simulation *with dead-bands* and with *no synthetic inertia*. We expect wide frequency deviations that repeatedly activate TGs. The obtained histogram is shown in Fig. 8 (magenta, ⓓ); in the same figure we report also the previous result with the variance equal to 1 MW. We easily see the almost flat portion of the magenta histogram and the bins located outside the dead-band. One could argue that this distribution tends to be bimodal. However, the study of

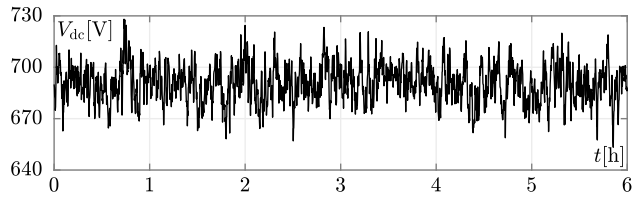

Fig. 7. The $V_{\rm dc}$ bus voltage in the schematic of Fig. 2. The nominal value of $V_{\rm dc}^{\rm ref}$ is 680 V; the maximum and minimum voltage limits are 680 ± 68 V.

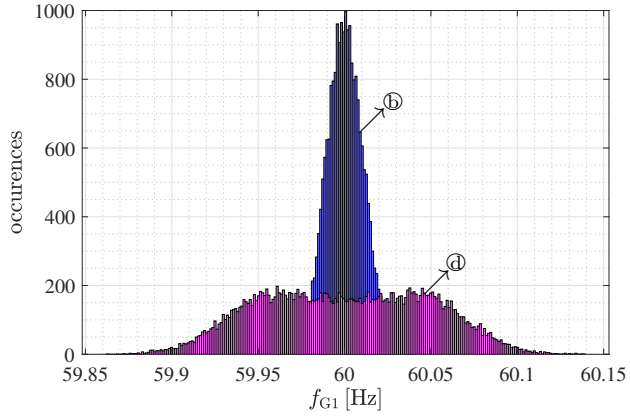

Fig. 8. Histograms of the frequency variations. The magenta histogram ⓓ refers to the scenario with *dead-bands*, *no synthetic inertia* and with the variance of the stochastic load raised at 10 MW. The blue histogram ⓑ is a replica of the blue one of Fig. 6.

the bimodal nature of frequency distribution is not trivial and involves analyses and hypotheses which are far beyond the scope of this paper. These issues have been addressed in [21]. In Fig. 9 we report the output of the dead-band block of the TG of the G1 generator. [2], [3]. We see a frequent activation of the TG. This makes almost useless the introduction of dead-bands, which basically worsen the frequency profile. Similarly to what observed in Fig. 6, the combined action of RESs coordination and synthetic inertia could significantly reduce TGs activity, even in case of more severe power variations.

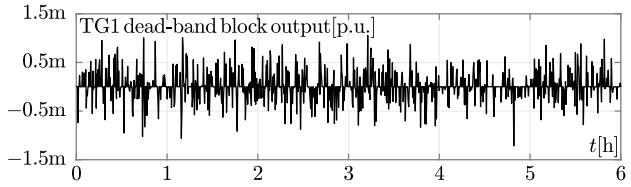

Fig. 9. The dead-band block output of the TG of G1 when the variance of the stochastic load amounts to 10 MW.

IV. Conclusion

In this paper we analyzed the effect of synthetic inertia provided by converter-interfaced generators on power systems. The paper addressed the potential beneficial effects of synthetic inertia provided by RESs-fuelled generators to compensate the natural imbalances between demand and generators. To this end, the converters interfacing RESs-fuelled generators with the AC grid should be made up of three stages: (i) a DC/DC converter which connects the solar panels to the second stage; (ii) a DC bus which hosts an energy storage device (a supercapacitor in the present work); and (iii) a bidirectional DC/AC converter which connects the previous stages to the AC grid. The control of the two converters has been modified in order to allow the system to mimic the inertial response of a synchronous generator. By introducing an equivalent PV generator in the IEEE 14-bus system and simulating the dynamic evolution of frequency in different scenarios, it has been shown that synthetic inertia allows to efficiently limit frequency variations caused by the presence of stochastically varying loads. This results in the beneficial decrease of the number of TGs interventions due to the trespassing of the dead-bands that are installed in their control scheme.

References

[1] N. W. Miller, K. Clark, and M. Shao, "Frequency responsive wind plant controls: Impacts on grid performance," in *2011 IEEE Power and Energy Society General Meeting*, Jul. 2011, pp. 1–8.

[2] North American Electric Reliability Corporation (NERC), *Frequency Response Initiative Report: The Reliability Role of Frequency Response*, 2012.

[3] ——, *2018 Frequency Response Annual Analysis*, 2018.

[4] J. Heres, W. van Westering, G. van der Lubbe, and D. Janssen, "Stochastic effects of customer behaviour on bottom-up load estimations," *CIRED - Open Access Proceedings Journal*, vol. 2017, no. 1, pp. 2543–2547, 2017.

[5] Q. Dai, T. Cai, S. Duan, and F. Zhao, "Stochastic modeling and forecasting of load demand for electric bus battery-swap station," *IEEE Trans. Power Del.*, vol. 29, no. 4, pp. 1909–1917, Aug. 2014.

[6] P. Vorobev, D. M. Greenwood, J. H. Bell, J. W. Bialek, P. C. Taylor, and K. Turitsyn, "Deadbands, Droop, and Inertia Impact on Power System Frequency Distribution," *IEEE Trans. Power Syst.*, vol. 34, no. 4, pp. 3098–3108, Jul. 2019.

[7] F. M. Mele, A. Ortega, R. Zárate-Miñano, and F. Milano, "Impact of variability, uncertainty and frequency regulation on power system frequency distribution," in *2016 Power Systems Computation Conference (PSCC)*, Jun. 2016, pp. 1–8.

[8] P. Tielens and D. Van Hertem, "The relevance of inertia in power systems," *Renewable and Sustainable Energy Reviews*, vol. 55, pp. 999–1009, 2016.

[9] U. Tamrakar, D. Shrestha, M. Maharjan, B. P. Bhattarai, T. M. Hansen, and R. Tonkoski, "Virtual inertia: Current trends and future directions," *Applied Sciences (Switzerland)*, vol. 7, no. 7, 2017.

[10] M. Dreidy, H. Mokhlis, and S. Mekhilef, "Inertia response and frequency control techniques for renewable energy sources: A review," *Renewable and Sustainable Energy Reviews*, vol. 69, pp. 144–155, 2017.

[11] A. Ademola-Idowu and B. Zhang, "Optimal design of virtual inertia and damping coefficients for virtual synchronous machines," in *IEEE Power & Energy Society General Meeting (PESGM)*, 2018, pp. 1–5.

[12] F. Milano and R. Zárate-Miñano, "A Systematic Method to Model Power Systems as Stochastic Differential Algebraic Equations," *IEEE Trans. Power Syst.*, vol. 28, no. 4, pp. 4537–4544, Nov. 2013.

[13] V. Bokharaie, R. Sipahi, and F. Milano, "Small-signal stability analysis of delayed power system stabilizers," in *2014 Power Systems Computation Conference*, 2014, pp. 1–7.

[14] F. Milano, *Power System Modelling and Scripting*. London: Springer, 2010.

[15] R. D. Christie, "Power system test archive," 1999, [Online]. Available at: https://labs.ece.uw.edu/pstca/.

[16] R. Singh, B. C. Pal, and R. A. Jabr, "Statistical Representation of Distribution System Loads Using Gaussian Mixture Model," *IEEE Trans. Power Syst.*, vol. 25, no. 1, pp. 29–37, Feb. 2010.

[17] P. Kundur, *Power system stability and control*. New York: McGraw-Hill, 1994.

[18] F. Bizzarri, A. Brambilla, G. Storti Gajani, and S. Banerjee, "Simulation of real world circuits: Extending conventional analysis methods to circuits described by heterogeneous languages," *IEEE Circuits Syst. Mag.*, vol. 14, no. 4, pp. 51–70, 2014.

[19] F. Bizzarri and A. Brambilla, "PAN and MPanSuite : Simulation vehicles towards the analysis and design of heterogeneous mixed electrical systems," in *Proceedings - 2017 1st New Generation of CAS, NGCAS 2017*, 2017, pp. 1–4.

[20] M. Liu, I. Dassios, G. Tzounas, and F. Milano, "Stability analysis of power systems with inclusion of realistic-modeling wams delays," *IEEE Trans. Power Syst.*, vol. 34, no. 1, pp. 627–636, Jan. 2019.

[21] D. del Giudice, A. Brambilla, S. Grillo, and F. Bizzarri, "Effects of Inertia, Load Damping and Dead-Bands on Frequency Histograms and Frequency Control of Power Systems," *Int. J. Elec. Power*, vol. 129, no. 106842, pp. 1–10, Jul. 2021.